View metadata, citation and similar papers at core.ac.uk

brought to you by CORE

provided by Purdue E-Pubs

Physics

Physics Research Publications

Purdue University *Year* 2008

Higgs decays and brane gravi-vectors

T. E. Clark B. Y. Liu S. T. Love

C. Xiong T. ter Veldhuis

This paper is posted at Purdue e-Pubs.
http://docs.lib.purdue.edu/physics_articles/1000

PHYSICAL REVIEW D **78,** 075016 (2008)

Higgs decays and brane gravi-vectors

T. E. Clark,* Boyang Liu,+ S. T. Love,‡ and C. Xiong§
Department of Physics, Purdue University, West Lafayette, Indiana 47907-2036, USA

T. ter Veldhuis‖
Department of Physics & Astronomy, Macalester College, Saint Paul, Minnesota 55105-1899, USA
(Received 10 June 2008; published 20 October 2008)

Higgs boson decays in flexible brane world models with stable, massive gravi-vectors are considered. Such vectors couple bilinearly to the standard model fields through either the standard model energy-momentum tensor, the weak hypercharge field strength, or the Higgs scalar. The role of the coupling involving the extrinsic curvature is highlighted. It is found that within the presently allowed parameter space, the decay rate of the Higgs into two gravi-vectors (which would appear as an invisible Higgs decay) can be comparable to the rate for any of the standard model decay modes.

DOI: 10.1103/PhysRevD.78.075016 PACS numbers: 14.80.Cp

Various theoretical extensions of theories of gravity include vector particles. In particular, such gravi-vectors [1] appear in flexible brane world models in which a four-dimensional space-time is embedded in a higher-dimensional space-time thus breaking the extra-dimensional spatial translation symmetries [2]. When these symmetries are made local thereby including higher-dimensional gravitational interactions, the erstwhile Nambu-Goldstone scalar degrees of freedom [3] associated with the higher-dimensional spatial translation symmetry breakdown become the longitudinal components of the now massive vector particles, X_i^μ. For $N \geq 2$ additional compactified isotropic spatial dimensions, these vectors, which are completely neutral under the standard model gauge group, carry an additional $SO(N)$ quantum number, labeled by $i = 1, \ldots, N$, which reflects the isometry of the codimensional space when the four-dimensional brane is embedded in the larger-dimensional space-time. On the other hand, all standard model particles are $SO(N)$ singlets. Consequently, $SO(N)$ invariant interactions of these vector Proca fields require them to appear in pairs and they are thus massive, stable physical degrees of freedom. For a single codimension, $N = 1$, the vector is stable provided there is a unbroken parity with respect to the extra dimension under which the brane vector is odd. Being stable, the vectors are also candidates for the dark matter of the Universe and are thus subject to the appropriate constraints [4].

The method of nonlinear realizations is a powerful tool which can be used to extract the generic form of vector interactions in a model independent given only the structure of the particular symmetry breakdown. In previous work [1], we applied this coset construction to the case of local space-time symmetries in brane world models. The resulting interaction terms of the resultant vector field will then contain various model-dependent parameters such as masses and dimensionless couplings which are not fixed by the method of nonlinear realizations but must be determined either using explicit models or by experiment. In the present case, the strength of the vector interactions is governed by the ratio $\frac{M_X^2}{F_X^4}$ where M_X is the vector mass whose nonzero value is model dependent and F_X^4 is the brane tension. In the flexible brane limit where the brane tension is much smaller than the D-dimensional Planck scale, the Kaluza-Klein modes of higher-dimensional gravity decouple from the standard model particles and thus we can focus attention on the coupling of the brane-vectors to the standard model. A Kaluza-Klein decomposition of higher-dimensional gravity has been performed [5] in this flexible brane world scenario and the properties of the extra vectors resulting from this decomposition were explored. The vector mass was found to be proportional to the exponential of the vacuum expectation value of the radion (dilaton) field reflecting its model-dependent magnitude.

The leading four-dimensional couplings of these vectors to the standard model are given by [4]

$$S_{X-\mathrm{SM}} = \int d^4x [\mathcal{L}_{TXX} + \mathcal{L}_{BXX} + \mathcal{L}_{HXX}]. \tag{1}$$

Here the effective Lagrangian

$$\mathcal{L}_{TXX} = \frac{1}{2} \frac{M_X^2}{F_X^4} X_i^\mu T^{\mathrm{SM}}_{\mu\nu} X_i^\nu \tag{2}$$

details the coupling of the induced metric on the brane to the standard model symmetric energy-momentum tensor $T^{\mathrm{SM}}_{\mu\nu}$. The other two interactions involve the extrinsic curvature and vector field strength tensors. The extrinsic curvature tensor

*clark@physics.purdue.edu
+liu115@purdue.edu
‡love@physics.purdue.edu
§xiong@purdue.edu
‖terveldhuis@macalester.edu

 © 2008 The American Physical Society

$$K_i^{\mu\nu} = \tfrac{1}{2}(\partial^\mu X_i^\nu + \partial^\nu X_i^\mu) + \ldots \tag{3}$$

measures the curvature of the embedded brane relative to enveloping D-dimensional geometry, while the vector field strength is given by

$$X_i^{\mu\nu} = \partial^\mu X_i^\nu - \partial^\nu X_i^\mu. \tag{4}$$

The product of the extrinsic curvature tensor and field strength couple to the standard model singlet weak hypercharge field strength $B_{\mu\nu} = \partial_\mu B_\nu - \partial_\nu B_\mu$ with $B_\mu = \cos\theta_W A_\mu - \sin\theta_W Z_\mu$ as

$$\mathcal{L}_{BXX} = \frac{M_X^2}{2F_X^4}[\kappa_1 B_{\mu\nu} + \kappa_2 \tilde{B}_{\mu\nu}]X_i^{\mu\rho} K_{i\nu}^{\rho}. \tag{5}$$

The coefficients κ_1, κ_2 are dimensionless constants of the effective Lagrangian. Finally, there is an invariant coupling to the standard model scalar doublet bilinear, $\phi^\dagger\phi$, given by

$$\mathcal{L}_{HXX} = \frac{M_X^2}{2F_X^4}[\lambda_1 K_i^{\mu\nu} K_{i\mu\nu} + \lambda_2 X_{i\mu\nu} X_i^{\mu\nu} + \lambda_3 X_{i\mu\nu}\tilde{X}_i^{\mu\nu}] \times \left(\phi^\dagger\phi - \frac{v^2}{2}\right), \tag{6}$$

with $v^2 = \frac{M_W^2 \sin^2\theta_W}{\pi\alpha}$. In unitary gauge, $\phi^\dagger\phi - \frac{v^2}{2} = vH + \frac{1}{2}H^2$ with H the Higgs scalar so that included in $\mathcal{L}_{HXX}$ is the interaction of the Higgs to two X fields. Here again, the coefficients λ_1, λ_2, λ_3 are dimensionless constants of the effective Lagrangian.

Thus the effective interaction (1) is characterized by two mass scales, F_X and M_X, which we treat as free parameters as well as five model-dependent dimensionless couplings, κ_1, κ_2, λ_1, λ_2, λ_3. Constraints on the $F_X - M_X$ parameter space have been obtained [4] using collider data and dark matter limits. For the numerical estimates made in this paper, we shall, for definiteness, use the value $F_X = 250$ GeV which is well within the currently allowed range for $M_X \leq 100$ GeV and is appropriate for a Higgs boson with mass less than 200 GeV. Moreover, for definiteness, we take $N = 2$.

We now turn to consider Higgs boson decays containing a pair of X vectors. We begin with the decay $H \to XX$ which appears as an invisible Higgs decay. The leading order Feynman graph for this process is displayed in Fig. 1 where the vertex is secured using the effective Lagrangian $\mathcal{L}_{HXX}$. Note that $\mathcal{L}_{TXX}$ does not contribute to the leading order graph since vacuum stability dictates that there is no term linear in H in the Higgs potential. The decay rate is readily computed as

$$\Gamma(H \to XX) = \frac{N\sin^2\theta_W}{32\pi^2\alpha}\frac{M_H^7 M_W^2}{F_X^8}\sqrt{1-4\xi^2} \times \left[\left(\frac{\lambda_1}{4} + \lambda_2\right)^2 (1-2\xi^2)^2\left(\frac{1}{4} - \xi^2 + 3\xi^4\right) + \left(\frac{\lambda_1^2}{16} - \lambda_2^2\right)\frac{1}{2}(1-2\xi^2)^2(1-4\xi^2) + \frac{1}{4}\left(\frac{\lambda_1}{4} - \lambda_2\right)^2(1-4\xi^2)^2 + 8\lambda_3^2\xi^4(1-4\xi^2)\right], \tag{7}$$

with $\xi \equiv \frac{M_X}{M_H}$. Figures 2 and 3 display the ratio of this rate to the total Higgs decay rate as computed in the standard model for Higgs masses of 120 GeV and 180 GeV taking the parameters $\lambda_1 = \lambda_2 = \lambda_3 = 1$.

We see that the rate of Higgs decay to a pair of X vectors for these parameters is quite comparable to the rate for any of the standard model decay channels. Note that the F_X dependence is quite steep varying as $1/F_X^8$. Even so, for an F_X value as high as 500 GeV, the 120 GeV Higgs boson will still decay to the X pairs at roughly a rate of 10^{-3} that obtained from the standard model.

Since the Higgs decay to $\mu\bar{\mu}$ is one of considerable focus at the LHC, we next consider the decay channel $H \to \mu\bar{\mu}XX$ which would appear as $\mu\bar{\mu}$ plus missing energy. This process can be mediated by either the induced metric coupling $\mathcal{L}_{TXX}$ to the energy-momentum tensor $T_{\mu\nu}^{\rm SM}$ or the coupling $\mathcal{L}_{BXX}$ to the weak hypercharge. The former interactions appear in the Feynman graphs of Fig. 4. The

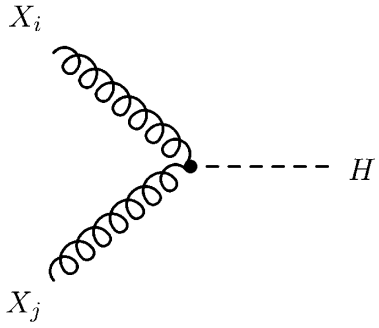

FIG. 1. Leading order Feynman graph for process $H \to XX$.

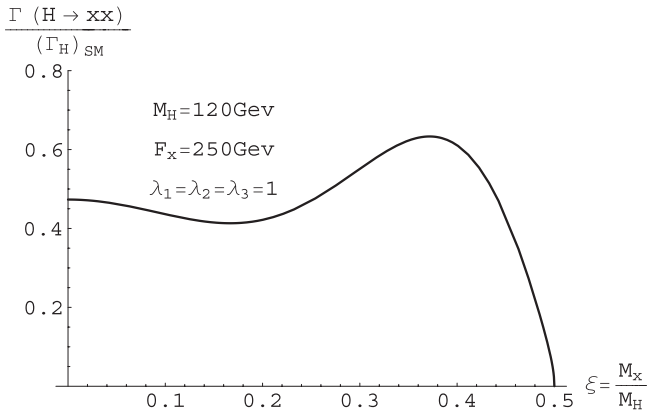

FIG. 2. Ratio of decay rate for $H \to XX$ to the standard model Higgs decay rate as a function of M_X/M_H with $M_H = 120$ GeV and $F_X = 250$ GeV.

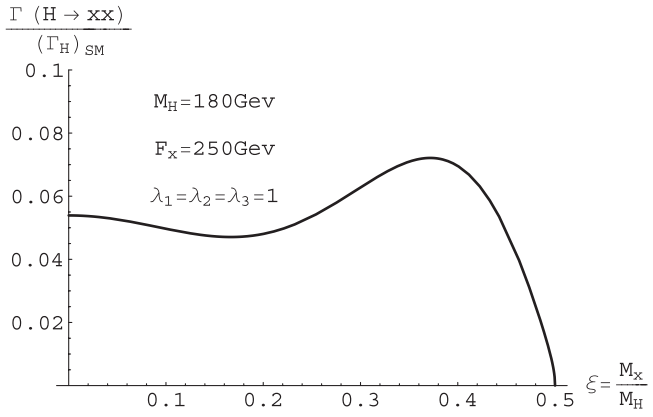

FIG. 3. Ratio of decay rate for $H \rightarrow XX$ to the standard model Higgs decay rate as a function of M_X/M_H with $M_H = 180$ GeV and $F_X = 250$ GeV.

amplitude obtained from these graphs varies as $\frac{m_\mu}{F_X^4}$ and is thus, in general, suppressed relative to the amplitude obtained from the graph of Fig. 5 which depends on the extrinsic curvature coupling $\mathcal{L}_{BXX}$ and is independent of m_μ.

In Figs. 6 and 7 the ratio is plotted of the total rate for this process to the standard model rate of Higgs decay to $\mu\bar{\mu}$ for a Higgs mass of 120 GeV while taking $\kappa_1 = \kappa_2 = 1$. The rather sharp peak in Fig. 6 arises when both of the internal Z lines are basically on shell thus providing a significant enhancement. For this narrow range of M_X masses which is roughly centered about $M_X \simeq 13$ GeV, the ratio is $\sim 10^{-3}$. It then falls quite dramatically by several orders of magnitude as seen in the Fig. 7. The bump in this plot arises from one of the internal Z lines being essentially on shell. This generic type of behavior is also seen for a Higgs mass of 180 GeV as evidenced in the Fig. 8. Once again, there is a narrow range of M_X values where the decay rate $\Gamma(H \rightarrow \mu\bar{\mu}XX)$ relative to the stan-

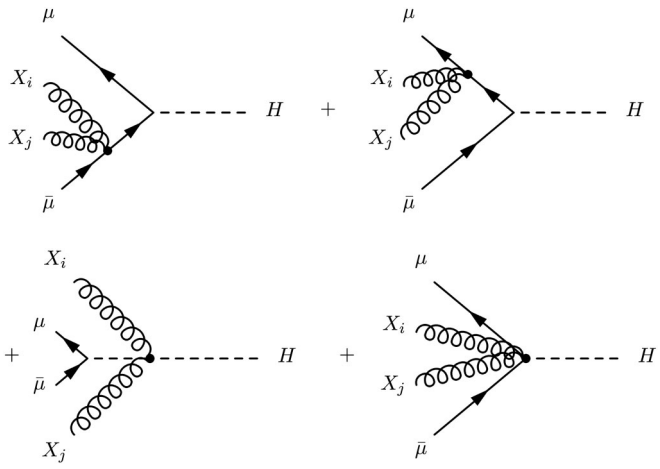

FIG. 4. Leading order Feynman graphs for the decay $H \rightarrow \mu\bar{\mu}XX$ mediated using the coupling $\mathcal{L}_{TXX}$.

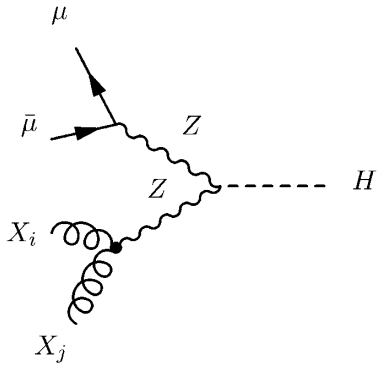

FIG. 5. Leading order Feynman graph for the decay $H \rightarrow \mu\bar{\mu}XX$ mediated using the coupling $\mathcal{L}_{BXX}$.

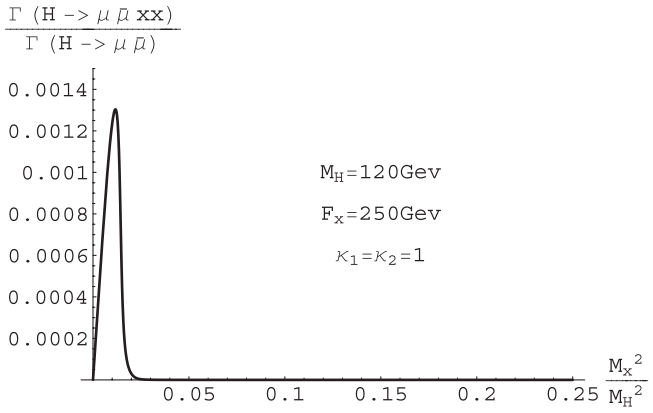

FIG. 6. Ratio of decay rate for $H \rightarrow \mu\bar{\mu}XX$ to standard model rate for $H \rightarrow \mu\bar{\mu}$ as a function of M_X^2/M_H^2 for $M_H = 120$ GeV and $F_X = 250$ GeV with the scale on the vertical axis appropriate for displaying the sharp peak at $M_X \simeq 13$ GeV.

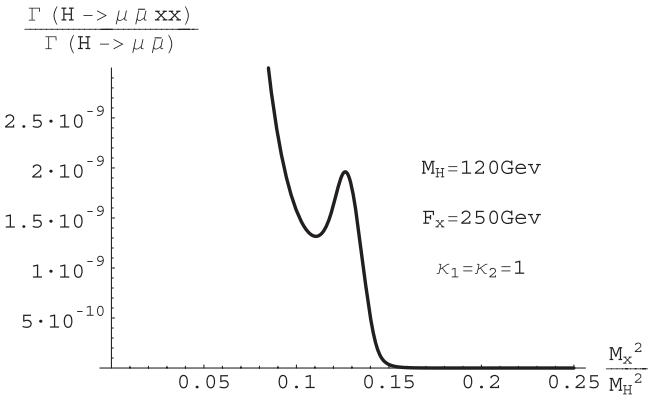

FIG. 7. Ratio of decay rate for $H \rightarrow \mu\bar{\mu}XX$ to standard model rate for $H \rightarrow \mu\bar{\mu}$ as a function of M_X^2/M_H^2 for $M_H = 120$ GeV and $F_X = 250$ GeV with the scale on the vertical axis appropriate for displaying a secondary, much lower peak at $M_X^2/M_H^2 \simeq 0.13$.

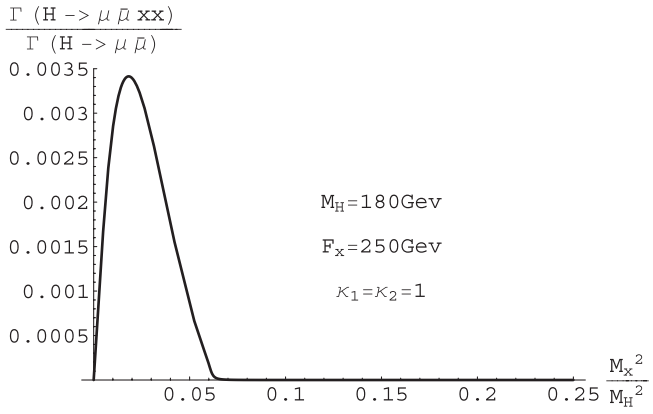

FIG. 8. Ratio of decay rate for $H \to \mu\bar{\mu}XX$ to standard model rate for $H \to \mu\bar{\mu}$ as a function of M_X^2/M_H^2 for $M_H = 180$ GeV and $F_X = 250$ GeV with the scale on the vertical axis appropriate for displaying the dominant peak.

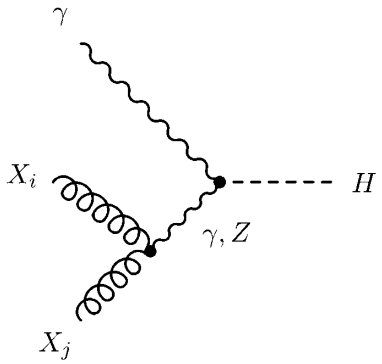

FIG. 9. Leading order Feynamn graph for the process $H \to \gamma XX$.

dard model rate for $H \to \mu\bar{\mu}$ is a few parts in 10^{-3} while for other M_X values the ratio steeply drops to an experimentally inaccessible range.

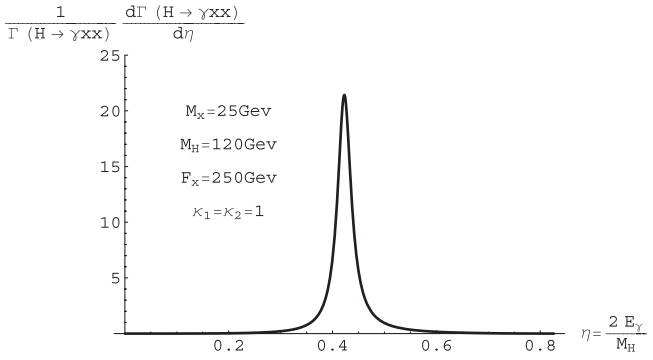

FIG. 10. Ratio of differential rate $\frac{d\Gamma(H\to\gamma XX)}{d\eta}$, with $\eta = \frac{2E_\gamma}{M_H}$, to total rate for $H \to \gamma XX$ as a function of η.

Finally, we consider the decay rate $H \to \gamma XX$ which appears as a photon plus missing energy. The leading Feynman graph contributing to this process is displayed in Fig. 9.

Here for the $H\gamma\gamma$ and $H\gamma Z$ vertices, we use the 1-loop standard model effective couplings

$$S_{H\gamma\gamma} + S_{H\gamma Z} = \frac{\sin^2\theta_W M_W^2}{\sqrt{4\pi M_H^3}} \int d^4x \left[\sqrt{\Gamma_{H\to\gamma\gamma}} F_{\mu\nu}F^{\mu\nu}H + \sqrt{\frac{2\Gamma_{H\to\gamma Z}}{(1-\frac{M_Z^2}{M_H^2})^3}} F_{\mu\nu}Z^{\mu\nu}H \right], \tag{8}$$

with $F_{\mu\nu} = \partial_\mu A_\nu - \partial_\nu A_\mu$; $Z_{\mu\nu} = \partial_\mu Z_\nu - \partial_\nu Z_\mu$ which is secured from the fermion and W vector 1-loop graphs. On the other hand, the γXX and ZXX vertices are given by the effective Lagrangian $\mathcal{L}_{BXX}$. The doubly differential decay rate $\frac{d\Gamma(H\to\gamma XX)}{dE_\gamma d\Omega_\gamma}$ is isotropic in the Higgs rest frame, while the differential rate with respect to photon energy in this frame takes the form

$$\frac{d\Gamma(H\to\gamma XX)}{dE_\gamma} = \frac{N}{384\pi^3}\frac{M_X^2 M_H^5}{F_X^8}\eta^3(1-\eta)^{3/2}\left(1-\eta-\frac{4M_X^2}{M_H^2}\right)^{3/2}\left[\kappa_1^2(1-\eta)+\kappa_2^2\left(1-\eta-\frac{4M_X^2}{M_H^2}\right)\right]$$
$$\times\left\{\frac{4\cos^2\theta_W}{(1-\eta)^2}\Gamma_{H\to\gamma\gamma} - \frac{4\cos\theta_W\sin\theta_W(1-\eta-\frac{M_Z^2}{M_H^2})}{(1-\eta)[(1-\eta-\frac{M_Z^2}{M_H^2})^2+\frac{M_Z^2\Gamma_Z^2}{M_H^4}]}\sqrt{\frac{2\Gamma_{H\to\gamma\gamma}\Gamma_{H\to\gamma Z}}{(1-\frac{M_Z^2}{M_H^2})^3}}\right.$$
$$\left. + \frac{2\sin^2\theta_W}{[(1-\eta-\frac{M_Z^2}{M_H^2})^2+\frac{M_Z^2\Gamma_Z^2}{M_H^4}]}\frac{\Gamma_{H\to\gamma Z}}{(1-\frac{M_Z^2}{M_H^2})^3}\right\}, \tag{9}$$

where $0 \le \eta = \frac{2E_\gamma}{M_H} \le 1 - \frac{4M_X^2}{M_H^2}$. In Fig. 10, we plot the ratio of the differential rate to the total rate for this process as a function of $\eta = \frac{2E_\gamma}{M_H}$ for $M_X = 25$ GeV, while Fig. 11 shows the ratio of the total rate for this process to the standard model rate for $H \to \gamma\gamma$.

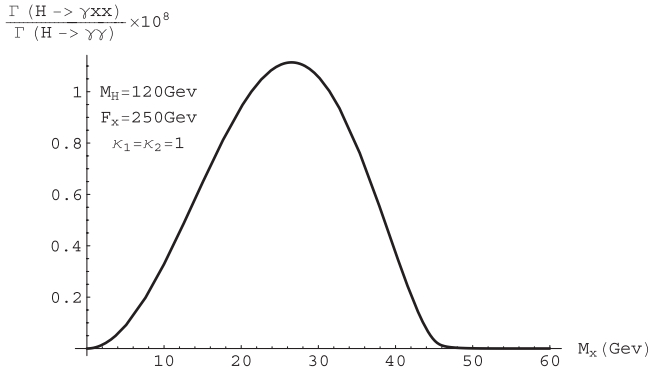

FIG. 11. Ratio of total rate for $H \rightarrow \gamma XX$ to standard model rate for $H \rightarrow \gamma\gamma$ as a function of M_X.

The peak tracks the enhancement accompanying the internal Z line going to mass shell. Unfortunately, the rate for this process is too small to allow for experimental detection.

A variety of flexible brane world models contain massive, stable vector fields [1,6]. In this paper we focused on the decay modes of the Higgs boson which contain a pair of such vectors. Using representative values of the vector effective Lagrangian parameters which are consistent with the current experimental limits, we found that the rate for $H \rightarrow XX$ (an invisible Higgs decay) could prove comparable to any of the standard model Higgs decay rates. Note that the invisible decay of the Higgs with comparable rates also occurs in other extensions of the standard model with additional stable, neutral, weakly interacting particles such as neutralinos in supersymmetric extensions of the standard model [7].

The work of T. E. C., S. T. L., and C. X. was supported in part by the U.S. Department of Energy under Grant No. DE-FG02-91ER40681 (Task B). The work of T. tV. was supported in part by the Research Corporation. T. tV. would like to thank the theory group at Purdue University for its hospitality during his sabbatical leave.

[1] T. E. Clark, S. T. Love, M. Nitta, T. ter Veldhuis, and C. Xiong, Phys. Rev. D **75**, 065028 (2007); S. T. Love, J. Phys. A **40**, 7049 (2007); T. E. Clark, S. T. Love, M. Nitta, and T. ter Veldhuis, Phys. Rev. D **72**, 085014 (2005).

[2] T. E. Clark, S. T. Love, M. Nitta, T. ter Veldhuis, and C. Xiong, Phys. Rev. D **76**, 105014 (2007); T. E. Clark and S. T. Love, Phys. Rev. D **73**, 025001 (2006); S. T. Love, Mod. Phys. Lett. A **20**, 2903 (2005); T. E. Clark, S. T. Love, M. Nitta, and T. ter Veldhuis, J. Math. Phys. (N.Y.) **46**, 102304 (2005); J. Gomis, K. Kamimura, and P. West, Classical Quantum Gravity **23**, 7369 (2006); J. High Energy Phys. 10 (2006) 015.

[3] P. Creminelli and A. Strumia, Nucl. Phys. **B596**, 125 (2001); A. R. Cembranos, A. Dobado, and A. L. Maroto, J. Phys. A **40**, 6631 (2007).

[4] T. E. Clark, S. T. Love, M. Nitta, T. ter Veldhuis, and C. Xiong, arXiv:0709.4023; S. T. Love, J. Phys. Conf. Ser. **110**, 072022 (2008).

[5] T. E. Clark, S. T. Love, M. Nitta, T. ter Veldhuis, and C. Xiong, arXiv:0809.1083.

[6] M. Bando, T. Kugo, T. Noguchi, and K. Yoshioka, Phys. Rev. Lett. **83**, 3601 (1999); T. Kugo and K. Yoshioka, Nucl. Phys. **B594**, 301 (2001).

[7] R. M. Godbole, M. Guchait, K. Mazumdar, S. Moretti, and D. P. Roy, Phys. Lett. B **571**, 184 (2003); H. Davoudiasl, T. Han, and H. E. Logan, Phys. Rev. D **71**, 115007 (2005).